



Effect of pre-exposure on crack initiation life of a directionally solidified Ni-base superalloy

Ali P. Gordon^{a,*}, Richard W. Neu^{b,c}, David L. McDowell^{b,c}

^a Department of Mechanical, Materials and Aerospace Engineering, University of Central Florida, P.O. Box 162450, Orlando, FL 32816-2450, United States

^b The George W. Woodruff School of Mechanical Engineering, Georgia Institute of Technology, Atlanta, GA 30332-0405, United States

^c School of Materials Science and Engineering, Georgia Institute of Technology, Atlanta, GA 30332-0245, United States

ARTICLE INFO

Article history:

Received 6 February 2008

Received in revised form 1 July 2008

Accepted 24 July 2008

Available online 5 August 2008

Keywords:

Pre-exposure

Creep

Directionally solidified

Ni-base superalloy

Pre-strain

ABSTRACT

Blades and vanes are just two of several industrial gas turbine (IGT) components often subjected to long periods of elevated temperature before, during, and after high stress operating conditions. In these systems, cyclic loading is induced by repeated start-ups, firings, and shut-down ramps. Combinations of complex thermal and mechanical service conditions in the presence of aggressive reactants facilitate crack initiation via oxide spike formation. In the current study, the effect of pre-exposure on the oxide spiking damage mechanism and crack initiation life is characterized for a representative directionally solidified (DS) Ni-base superalloy, e.g. DS GTD-111. Comparisons of unexposed and pre-exposed samples reveal that 100 h of either creep pre-strain and/or thermal pre-exposure strongly influences the dominant damage mechanism that leads to crack initiation under subsequent fatigue cycling. A mechanistic model for crack initiation is modified to capture the influence of pre-exposure on life.

© 2008 Elsevier Ltd. All rights reserved.

1. Introduction

It is estimated that the cost needed to replace an entire row of blades on a single land-based gas-powered turbine is approximately \$1M and is carried out nearly every 6 years. In many instances, first and second stage blades are retired from operation with little to no visible damage [1]. One approach to lowering these costs is by improving the fidelity of life prediction modeling resulting in maximum utilization of components.

Blades cast from directionally solidified (DS) Ni-base superalloys have been designed for the most aggressive operating conditions with regard to mechanical (e.g. up to 500 MPa), thermal (e.g. up to 1200 °C), and environmental (e.g. gases rich in H₂S particles) conditions. One of several consequences of super-imposing mechanical cycling with dwell periods in an aggressive environment is microstructural damage via surface formation of numerous sharp microcracks [2–6]. As described by Neu and Sehitoglu [5], this so-called oxide spiking mechanism occurs under out-of-phase (OOP) thermomechanical fatigue (TMF) conditions. Gordon [2] found that spiking is also prevalent under isothermal low cycle fatigue (LCF) conditions with compressive dwell periods (i.e. compressive creep-fatigue) [2].

It can be argued that physically based approaches to modeling fatigue life allow for more accurate and robust life prediction than phenomenological models is their limited reliability to extrapolate beyond experimental results. An expression for the oxide spike length was developed from metallurgical analysis of thermomechanically fatigue-tested specimens and thermally exposed samples [4,6], i.e.,

$$h_{cr} = \left[\frac{B\Phi_{env}(K_{OX} + K_{GPD})}{\delta_0} \right] \frac{(\Delta\epsilon_m)^2}{(\dot{\epsilon}_m)^{-b}} t^\beta, \quad (1)$$

where B , β , b , and δ_0 are material constants determined from TMF and isothermal fatigue tests. The term t represents time, and $\Delta\epsilon_m$ and $\dot{\epsilon}_m$ refer to mechanical strain range and mechanical strain rate, respectively. The factor, Φ_{env} , depends on the ratio of the thermal and mechanical strain rates and their phasing. The averaged diffusivity constants, K_{OX} and K_{GPD} , separately describe the surface diffusion of the oxide and γ' -depleted zone, respectively, under non-isothermal cycling, and are defined by

$$K_j = \frac{1}{t_{tc}} \int_0^{t_{tc}} \Theta_j \exp\left(-\frac{Q_j}{RT(t)}\right) dt. \quad (2)$$

where $j = OX, GPD$. Also Φ accounts for the dependence of oxidation on absolute temperature, T , measured in K. The quantities t_{tc} and Q correspond to the total cycle time and the activation energy, respectively. The cyclic damage rate due to environmental mechanisms becomes

* Corresponding author. Tel.: +1 4078234986; fax: +1 4078230208.

E-mail address: apgordon@mail.ucf.edu (A.P. Gordon).

$$\frac{dD}{dN}\bigg|_{\text{env}} = \left[\frac{B\Phi_{\text{env}}(\bar{K}_{\text{h,ox}} + \bar{K}_{\text{h,\gamma'}})}{h_{\text{cr}}\delta_o} \right]^{\frac{1}{p}} \frac{2(\Delta\epsilon_m)^{\frac{2}{p}+1}}{(\dot{\epsilon}_m)^{1-\frac{1}{p}}}. \quad (3)$$

Here $\bar{K}_{\text{h,ox}}$ and $\bar{K}_{\text{h,\gamma'}}$ are averaged diffusivity constants. When several damage mechanisms are operative, the formulation in Eq. (3) is incorporated into a cumulative model along with other damage modules. For example, a fatigue crack propagation model accounting for fatigue, environmental, and creep damage was proposed by Miller et al. [7].

Turbine blades are commonly subjected to mechanical and/or thermal loading in the forms of unloaded start-up firings, unintentional overstrains, etc. prior to their service usage. Although these pre-exposures can potentially inflict damage on a component (e.g. altering the surface condition or deteriorating the microstructure), they are often neglected in calculations of fatigue life. The microstructural effects of brief, sustained thermal and mechanical pre-exposure on fatigue crack initiation life is characterized in this study. Based on the collaboration between metallurgical and lifting analyses, an analytical model for stress-assisted surface corrosion is developed. Test results introduced here are derived from a series of independent, but related, experiments conducted in Georgia Tech's Mechanical Properties Research Laboratory (MPRL).

2. Pre-exposure effects on fatigue

The subject of load sequence effects on fatigue life has received attention since the early 1980s. The damage curve approach (DCA) was originally developed by Manson and Halford [8,9]. In this approach, the damage fraction for a two-level fatigue test was used to account for sequence effects, i.e.,

$$D = \left(\frac{n_1}{N_1} \right)^P + \left(\frac{n_2}{N_2} \right), \quad (4)$$

where N_1 and N_2 are the fatigue lives at the first and second load levels, n_1 is the number of cycles applied in the first level, and n_2 is the number of remaining cycles in the second level. The exponent P is a function of stress level that falls in the range of 0 and 1. Pre-straining effects on the PC superalloy IN-718 were investigated at room temperature (RT) [10]. To convert creep pre-strain data into equivalent fatigue pre-strain data, n_1 was assumed to be a quarter cycle with a strain range equal to twice the magnitude of the pre-strain. It was observed that compressive pre-straining up to 2% and at RT has virtually no effect on fatigue life.

Prior deformation at low ambient temperatures lowers creep resistance in single crystal (SC) and polycrystalline (PC) Ni-base superalloys because it introduces a high density of mobile dislocations [11–13]. At high temperatures, precipitate particle rafting of a SC Ni-base material with prior creep in vacuum affects crack propagation behavior [13]. During prior creep in compression, raft structures formed parallel to the stress axis hinder crack propagation transverse to the stress axis; furthermore, these rafts force cracks to meander out of their plane. The consequence is slightly longer fatigue life compared with samples that were not creep pre-strained. Conversely, rafts lying perpendicular to the stress axis develop from prior tensile creep facilitate crack propagation in subsequent fatigue and therefore lead to shorter lives. Compared to results in a vacuum, prior creep in air leads to the most drastic reduction to fatigue life, whereas lowering the temperature and/or removing all of the air from the environment affects life to a lesser extent [14]. It was later demonstrated that completely removing the surface-formed oxide layer via polishing mitigates the effect of environment [15].

The effect of prior high temperature exposure on the damage mechanisms and fatigue crack initiation life of a representative DS Ni-base superalloy (i.e., DS GTD-111) is the focus of the current

investigation. A variety of experiments are analyzed in order to characterize the dependence of life on creep pre-strain and high temperature pre-exposure. Comparisons are made with virgin samples with no prior loading or high temperature exposure. A physically based model for oxide spike depth based on Eqs. (1)–(3) is developed that can be incorporated in life prediction models.

3. Experimental method

The subject material of the current investigation is DS GTD-111. It has comparatively superior creep, fatigue, and corrosion resistance relative to polycrystalline (PC) Ni-base superalloys; hence it has been identified as a material of choice for first and second stage gas turbine blade designers. The chemical composition by weight of this DS Ni-base superalloy is listed in Table 1. The chemical composition and the grain structure of this material have been optimized to resist the harsh conditions common in gas turbine engines. This DS intermetallic consists of two phases, as shown in Fig. 1. The γ matrix phase is a solid solution strengthened FCC austenitic Ni. The L1₂-structured γ' precipitate phase is an ordered FCC super-lattice of nickel-aluminide, Ni₃Al, having a bimodal distribution. The cuboidal primary precipitates (0.5–1.0 μm) and spheroidal secondary precipitates (0.05–0.2 μm) occupy an overall volume fraction of approximately 46%. The γ' precipitates serve as the main strengthening phase [16]. In this columnar-grained material, void nucleation and grain boundary sliding are both limited since grain boundaries are not perpendicular to the primary stress direction of the blade. Test specimens were machined from longitudinal (L-oriented) and transverse (T-oriented) directions of a cast slab.

The types of elevated temperature experiments conducted on the L- and T-oriented DS samples were low cycle fatigue (LCF) with and without creep pre-strain and high temperature exposure. A summary of the fatigue tests is listed in Tables 2 and 3. Of the pre-exposed LCF-tested specimens, some were pre-exposed in unforced gases at high temperature with or without a statically applied load. To simulate the corrosive effects of the synthetic gas environment, several specimens were subjected to a sulfur-rich pre-exposure without load. This so-called syngas environment is produced from the integrated gasification combined cycle (IGCC), which is an efficient and clean approach to fossil fuel combustion [17]. This environment consists of gases of varying composition that are generated in coal gasification. Syngas consists primarily of carbon monoxide and hydrogen. It also contains sulfur compounds which are reactive with the turbine blade material. Pre-exposure consisted of a specified temperature (982 °C for all cases), mechanical load (0, ± 75 MPa, or ± 100 MPa), and environment (air or simulated syngas) for 100 h. Based on two prior studies on creep deformation and rupture [18] and stress-free oxidation kinetics [19], under these combinations of temperature, stress, and time, less than 10% of the creep rupture life will be exhausted and the accumulated oxidation layer will measure nearly 10 μm , respectively.

Pre-exposure in the simulated syngas environment was conducted using N₂ with 100 ppm H₂S at CC Technologies (Dublin, OH). In the stressed cases that were carried out on the servo-hydraulic MTS load frame assembly, creep deformation occurred and was digitally recorded. The specimens were subsequently tested under LCF conditions to determine the effect of pre-expo-

Table 1
Nominal chemical (wt%)

Material	Cr	Co	Ti	W	Al	Mo	Ta	C	Zr	B	Ni
DS Ni-base	14.0	9.5	4.9	3.8	3.0	1.6	2.8	0.10	0.02	0.01	Bal.

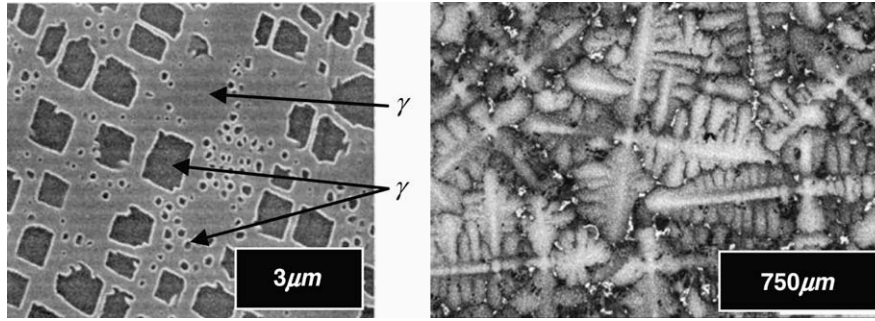


Fig. 1. Images of (left) the matrix and coarse and fine precipitate phases of a DS Ni-base superalloy and (right) dendritic structure.

sure on fatigue crack initiation life. For this investigation, the cycle during which the stabilized, maximum tensile load from initial cycling data dropped 20% is used to define the crack initiation life.

It should be noted that long and narrow test samples are preferred for creep deformation and rupture experimentation [20]. The dimensions of the test sample used in this study are appropriate for both early creep deformation as well as fatigue testing. Specimens have gage section lengths of 12.7 mm and gage section diameters of 6.35 mm. Since a highly accurate, direct contact extensometer was employed to measure strain, early creep deformation measurements were obtained. Data from creep rupture and deformation tests that were conducted in an earlier study are also relevant to the current investigation. These tests were performed

on a creep frame appropriate for long term creep deformation and rupture by Ibanez [18] in accordance with an ASTM standard E139 (2007) [20]. To support the development of the oxide spike depth model, results from stress-free thermal exposure experiments were used [19,21].

4. Effect of pre-exposure on microstructure

The most conspicuous effects of exposing Ni-base superalloys to high temperature conditions, either with or without pre-loading, can be categorized as those affecting either the surface or the sub-surface of the microstructure. When the DS material is exposed to 982 °C for 100 h in static laboratory air, an oxide layer measuring approximately 11 μm forms on the surface of the material [19]. Varying the exposure temperature and time significantly affects the oxidation penetration of the subject material [21]. Once the sample is subjected to subsequent mechanical loading, oxide spallation occurs, as shown in Fig. 2. The presence of the oxide layer prior to fatigue cycling alters the diffusion and damage processes local to the surface and influences the mechanisms of crack initiation.

The effects of prior high temperature exposure on fatigue crack initiation behavior of the L- and T-oriented DS samples were investigated using a standard pre-exposure time, $t_{pre} = 100$ h, and temperature, $T_{pre} = 982$ °C (cf. Table 3). While most specimens were pre-exposed in static air, two specimens were exposed to wet H₂S that simulated the gasified operating environment of the DS turbine blades. Additionally, while most specimens were pre-exposed with no stress, several were subjected to static pre-stress of either 100 MPa in tension or compression. Afterwards, each sample was

Table 2
Crack initiation life of L and T-oriented DS GTD-111 at 871 °C

Plastic strain range, $\Delta\epsilon_{pl}$ (%)	Elastic strain range, $\Delta\epsilon_{el}$ (%)	Crack initiation life, N_i	Specimen ID (orientation)
<0.01	0.50	29,159	L8-3 (L)
0.01	0.79	3699	GTD-CC04 (L)
0.08	0.82	987	A27-L-F6 (L)
0.03	0.97	1357	GTD-CC05 (L)
0.99	1.01	103	B17-L-F5
2.810	1.19	11	L8-2A (L)
<0.01	0.50	16,069	T8-2A (T)
0.07	0.73	598	T8-5 (T)
0.22	0.68	271	B17-T-F2 (T)
0.22	0.78	300	T8-2 (T)
1.46	0.54	28	T8-1A (T)
2.87	1.13	3	T8-1 (T)

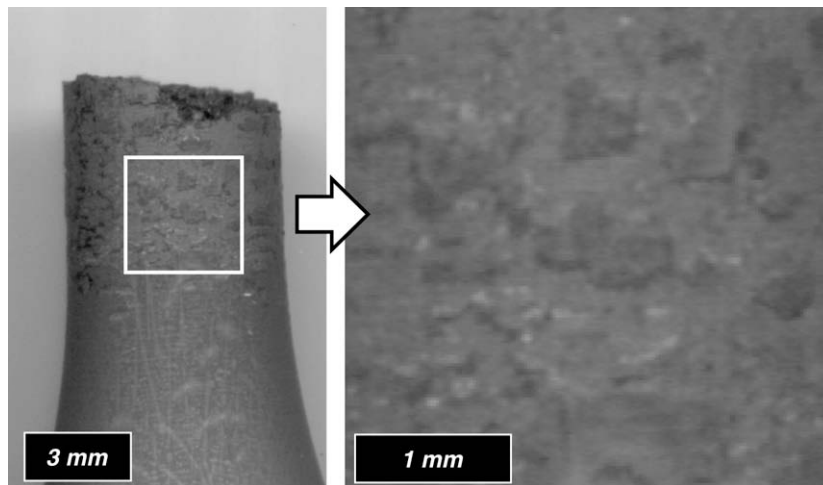


Fig. 2. Oxide spallation after LCF cycling of a compressively pre-crept (982 °C, $t_{pre} = 100$ h, 0 MPa, air) L-oriented DS specimen.

Table 3
Crack initiation life of pre-exposed DS GTD-111 (for each case $t_{pre} = 100$ h)

Pre-exposure			Fatigue test						
Temperature, T (°C)	Environment	Load (MPa)	Temperature, T (°C)	Environment	Total strain range, $\Delta\epsilon_m$ (%)	Plastic strain range, $\Delta\epsilon_{pl}$ (%)	Elastic strain range, $\Delta\epsilon_{el}$ (%)	Crack initiation life, N_i	Specimen ID (orientation)
982	Air	100	871	Air	0.80	0.22	0.58	167	A27-L-F1 (L)
982	Air	100			Creep deformation too large				A27-L-F2
982	Air	-100	871	Air	0.80	<0.01	0.80	1857	A27-L-F8 (L)
982	Air	-100			Specimen buckled under compression				L8-12A (L)
982	Air	-100			Specimen buckled under compression				A27-L-F11
No pre-exposure			871	Air	0.50	<0.01	0.50	29159	L8-3 (L)
982	Air	0	871	Air	0.50	0.05	0.45	4250	B18-L-F6 (L)
No	Pre-exposure		871	Air	0.80	0.01	0.79	3699	GTD-CC04 (L)
982	Air	0	871	Air	0.80	<0.01	0.80	1958	B17-L-F3 (L)
982	Wet H ₂ S	0	871	Air	0.80	0.23	0.57	979	A27-L-F15 (L)
982	Air/ polished	0	871	Air	0.80	0.03	0.77	1601	L8-12 (L)
No pre-exposure			871	Air	0.50	<0.01	0.50	16069	T8-2A (T)
982	Air	0	871	Air	0.50	0.04	0.46	548	B17-T-F5 (T)
No pre-exposure			871	Air	0.80	0.07	0.73	598	T8-5 (T)
982	Air	0	871	Air	0.80	0.16	0.64	221	A27-T-F5 (T)
982	Wet H ₂ S	0	871	Air	0.80	0.11	0.69	84	A27-T-F4 (T)

continuously fatigue cycled according to the test configurations listed in Table 2. A temperature of 871 °C, with $R_\epsilon = -1$ and $\dot{\epsilon} = 0.5\%/s$ was applied for all cases for fatigue loading.

Pre-exposing the subject material in either laboratory air or H₂S alters the surface of the material, as shown in Fig. 3. The crack initiation behavior of the material is not only influenced by the cumulative oxide layer, but also the γ' -depleted zone. The presence of the oxide layer, in locations where it has not spalled, protects the material from further oxidation. Nickel-base superalloys are known to passivate in this manner [19]. Also during fatigue cycling, the ductile γ' -depleted zone, which is essentially a matrix layer containing fine Ni₃Al particles [2], forms wide cracks that arrest upon reaching virgin material. At room temperature, the γ' -depleted zone was found to have a Vickers hardness that was less than that of the unaffected material [2]. The stress concentrations at these early-formed crack tips initiate the oxide spiking damage mechanism. Under identical strain-controlled LCF conditions without prior exposure, the oxide spiking damage mechanism does not occur. Pre-exposing the material in the H₂S environment led to deeper ingress of both layers compared to the air-exposed case. In both cases shown in Fig. 3, surface-initiated cracking was the dominant mechanism facilitating damage. Multiple hairline cracks emanated from early-formed matrix cracks and extended into the bulk of the material. Very little oxidation formed on the fracture surface in either case since the cracks advanced quickly and the temperature during fatigue was lowered. Since surface degradation was more aggressive in the H₂S-exposed case, the cracks in the γ' -denuded layer are longer.

In a previous study involving pre-exposure, it was demonstrated that removing both oxide and matrix layers via machining prior to high temperature fatigue cycling eliminated the life reduction effect for René 80 [15]. To characterize the individual roles of the surface layers, the oxide layer of an air-exposed DS material sample was hand-polished to a depth of approximately 20 μm and subsequently fatigue-tested. The polishing completely removed the oxide layer, and the γ' -depleted zone was left intact. Based on microscopy, it was determined that the spacing between surface cracks in the air-exposed and air-exposed polished cases were comparable. The crack initiation life of the polished sample was also comparable to that of the unpolished specimen, as shown in Table 3. These two experiments, along with the observation from the prior study by Antolovich et al. [15] implies that the presence of the γ' -depleted zone developed via prior exposure has a significant effect on the subsequent fatigue life.

In each case of this series of pre-exposure experiments, fatigue crack initiation life was reduced by pre-exposure. Microscopy was conducted to characterize the underlying mechanisms responsible for the reduction in mechanical strain life of the pre-loaded cases. Fig. 4 compares the microstructures of the two pre-crept and fatigued samples to that of a sample that was pre-crept in tension, but not subjected to any fatigue cycling whatsoever. Common to the surface of each material is the accumulated oxidation layer. Oxides spalled from the majority of the surface area of the case of prior creep in compression (Fig. 4c). For the two cases of prior creep in tension (e.g. Fig. 4a and b), numerous microcracks were found beneath the surface in a sample that was cycled in fatigue and a sample that was not subjected to any additional loading. Upon fatigue cycling, cracks emanating from the surface coalesced with those initiated at the subsurface, thus creating a tortuous fracture path. These subsurface cracks do not form in the compressively pre-crept case; therefore, the crack initiation behavior is much like that of the pre-heated/unloaded cases.

Rafting occurred in each of the cases of prior creep. These raft-shaped particles measure five times the original length of the cuboidal precipitate particles. Transmission electron microscopy (TEM) is needed to precisely determine the effect of rafting on the deformation behavior of the material, and is left for future study.

5. Effect of pre-exposure on life

The effect of pre-exposure on the initial cyclic stress-strain response of the L-oriented DS material is compared with its unexposed response in Fig. 5. While the pre-exposure in air either unloaded (Fig. 5a) or loaded in compression (Fig. 5c) had negligible effects on the initial hysteresis loops, the specimens pre-exposed to the simulated IGCC environment (Fig. 5b) and tensile loading in air (Fig. 5d) showed significant effects. These inelastic strain range deviations from the benchmark conditions arise from the microstructural effects discussed in the previous section. The effects of pre-exposure on the mechanical properties of the DS material were also investigated. Data for the initial elastic moduli were obtained from the initial loading cycles. Pre-creeping L-oriented DS samples in tension lowers E by approximately 24%. This is due to the formation of the brittle oxide and soft matrix layers at the surface (Fig. 4a). Other forms of high temperature pre-exposure (e.g. no load, compression or IGCC) have marginal effects on the modulus of either the L- or T-oriented material. Air-exposed specimens

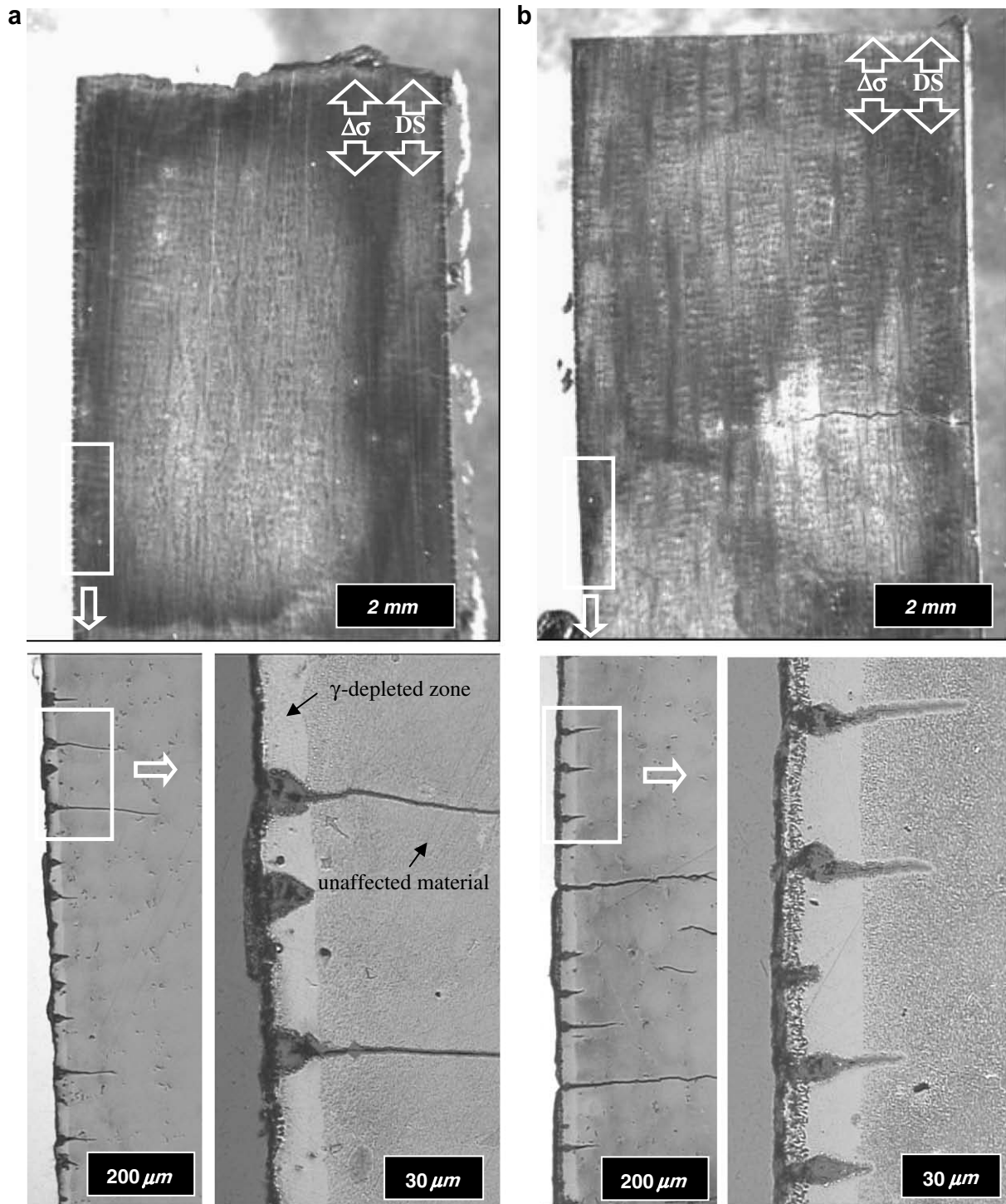


Fig. 3. Sequential exploded views of surfaces of test specimens of (a) air and (b) H₂S-exposed L-oriented DS samples. Pre-exposure conditions: 982 °C, 100 h, 0 MPa. Fatigue cycling conditions: $\Delta\epsilon = 0.8\%$ 871 °C, and $\dot{\epsilon} = 0.5\%/s$.

subjected to either 0 MPa or –100 MPa exhibit virtually no alteration of yield properties. Conversely, the materials pre-exposed in either tension or H₂S have lower yield strengths.

The effect of pre-exposure on the reduction of the crack initiation lives of the material is a direct consequence of the degraded microstructure and its mechanical properties. Fig. 6 shows the effect of pre-exposure on life. Of all of the unloaded cases considered with $\Delta\epsilon = 0.8\%$, pre-exposing the material in air has the least detrimental effect on life. Increasing the aggressive nature of the pre-

exposure environment from air to H₂S had the effect of increasing the oxide penetration which further decreased life. These reductions were exhibited by both the L- and T-oriented specimens (Fig. 6a). Both sets of air-exposed and unloaded cases for L- and T-oriented specimens indicate that as the mechanical strain range is decreased, crack initiation lives diverge from the benchmark cases. As such, the effects of pre-exposure on life are likely to be more pronounced under high cycle fatigue (HCF) but otherwise identical test conditions. Conversely, the life response for

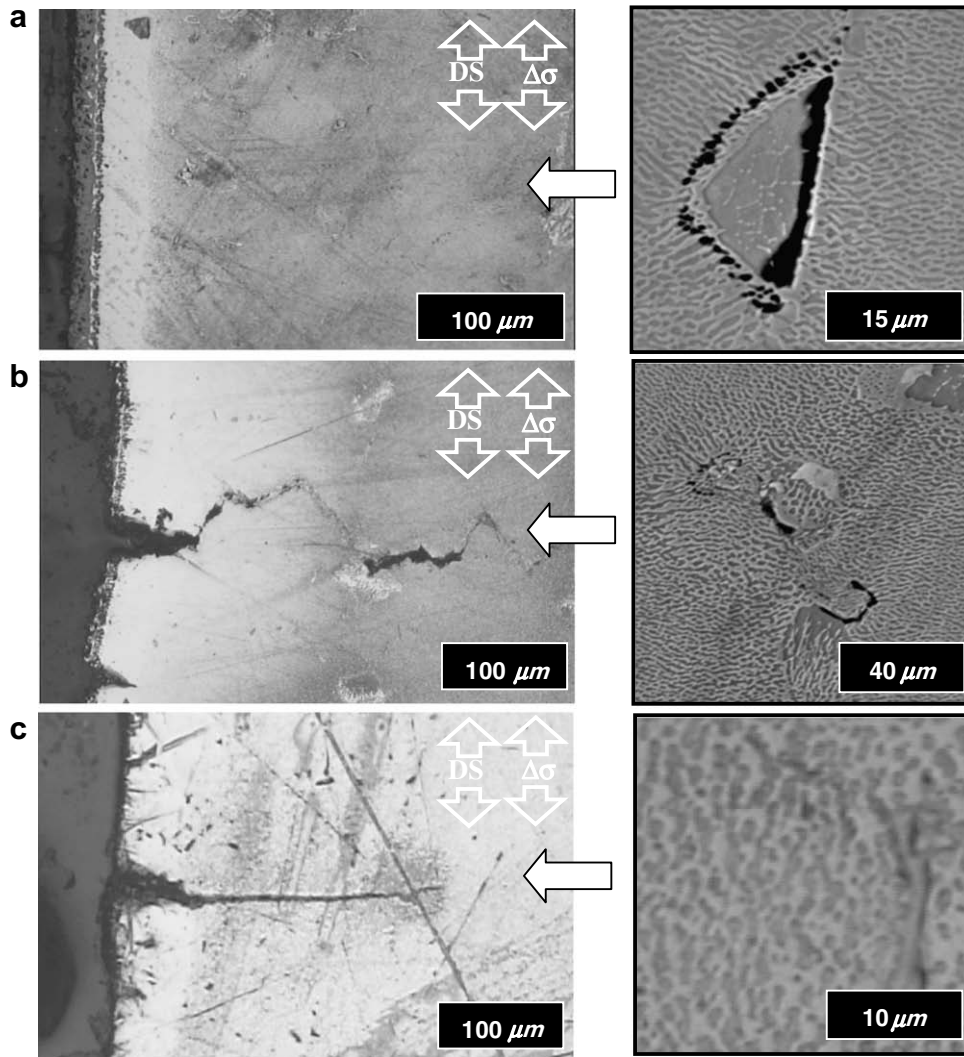


Fig. 4. Pre-exposure effects on crack initiation behavior of an L-oriented DS material in static air under (a) tensile pre-strain (100 h, 982 °C, 100 MPa) without subsequent fatigue, (b) tensile pre-strain (100 h, 982 °C, 100 MPa) and subsequent fatigue ($\Delta\varepsilon = 0.5\%$ and 871 °C), and (c) compressive pre-strain (100 h, 982 °C, 100 MPa) and subsequent fatigue ($\Delta\varepsilon = 0.8\%$ and 871 °C).

pre- and un-exposed samples should be nearly identical for the very low cycle fatigue (VLCF) [22] regime.

Pre-exposing the L-oriented material to either 0 MPa or -100 MPa in air had approximately an identical effect, a factor of two reduction in life. Formation of subsurface cracks caused by prior tensile creep, however, severely lowered the crack initiation life of the material compared to those samples not subjected to any prior exposure whatsoever (Fig. 6b).

6. Analytically modeling the effect of pre-exposure

Subjecting the DS samples to unstressed high temperature exposure in either laboratory air or simulated IGCC environments prior to fatigue cycling resulted in the development of surface layers (Fig. 4). Both the precipitate particle depleted zone and the oxide layer have distinct mechanical properties from those of the unaffected material. Upon cycling, cracks initiating from the surface rapidly propagate through the oxides and γ' -depleted region. After this initial period, continued crack growth occurs by way of the oxide spiking mechanism. Compared to unexposed samples, as in Table 3, pre-developed oxide layers severely shorten the fatigue life by initiating the oxidation and rupture processes at the

surface of the material. This “head start” can be represented graphically in terms of cyclic oxide rupture, as shown in Fig. 7. Instead of initiating from the origin, the oxide growth and cyclic rupture kinetics begin where the pre-exposure ends, i.e., the point $(t_{\text{pre}}, h_{\text{pre,ox}} + h_{\text{pre,GPD}})$. Here t_{pre} is the pre-exposure time and $h_{\text{pre,ox}}$ and $h_{\text{pre,GPD}}$ are the thicknesses of the oxide layer and γ' -depleted zone after pre-exposure, respectively, i.e.,

$$\begin{aligned} h_{\text{pre,ox}} &= \Theta_{\text{OX}}(T_{\text{pre}}, F_{\text{O}_2,\text{pre}})(t_{\text{pre}})^m \\ h_{\text{pre,GPD}} &= \Theta_{\text{GPD}}(T_{\text{pre}}, F_{\text{O}_2,\text{pre}})(t_{\text{pre}})^m \end{aligned} \quad (5)$$

The quantities “pre” on T_{pre} and t_{pre} denote the temperature and length of the pre-exposure period, respectively. Based on prior the stress-free oxidation studies [19,21], a good approximation for the surface layer depths developed by high temperature pre-exposure is based on the summation of both the accumulated oxidation and precipitate particle depleted zone layers, i.e.,

$$2h_{\text{pre}} \approx h_{\text{pre,OX}} + h_{\text{pre,GPD}}. \quad (6)$$

Consequently, the power law relationship used to develop an expression for h_{cr} in Eq. (1) can be re-written as

$$(h_{\text{cr}} - 2h_{\text{pre}}) = g[(t - t_{\text{pre}})]^\beta, \quad (7)$$

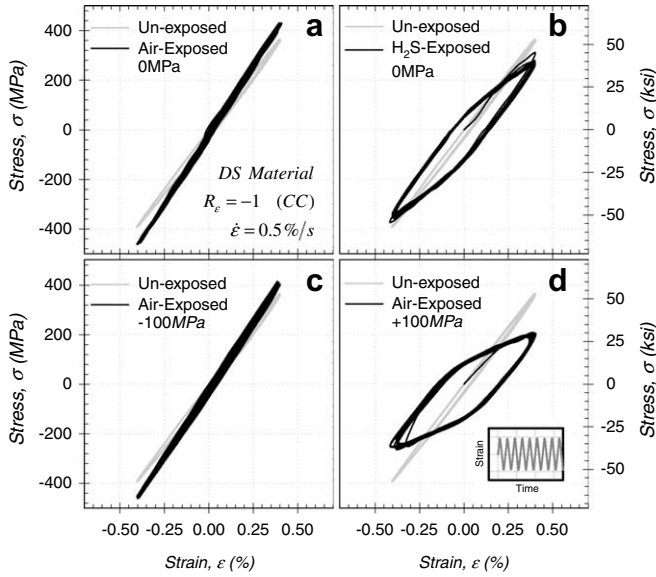


Fig. 5. Pre-exposure effects on initial hysteresis loops of L-oriented DS material under continuous cycling conditions with $R_e = -1$, $\dot{\epsilon} = 0.5\%/s$, and 871 °C (1600 °F): (a and b) pre-heated without pre-load and (c and d) simultaneously pre-heated and pre-loaded. For each pre-exposed case $T = 982$ °C (1800 °F) and $t_{pre} = 100$ h.

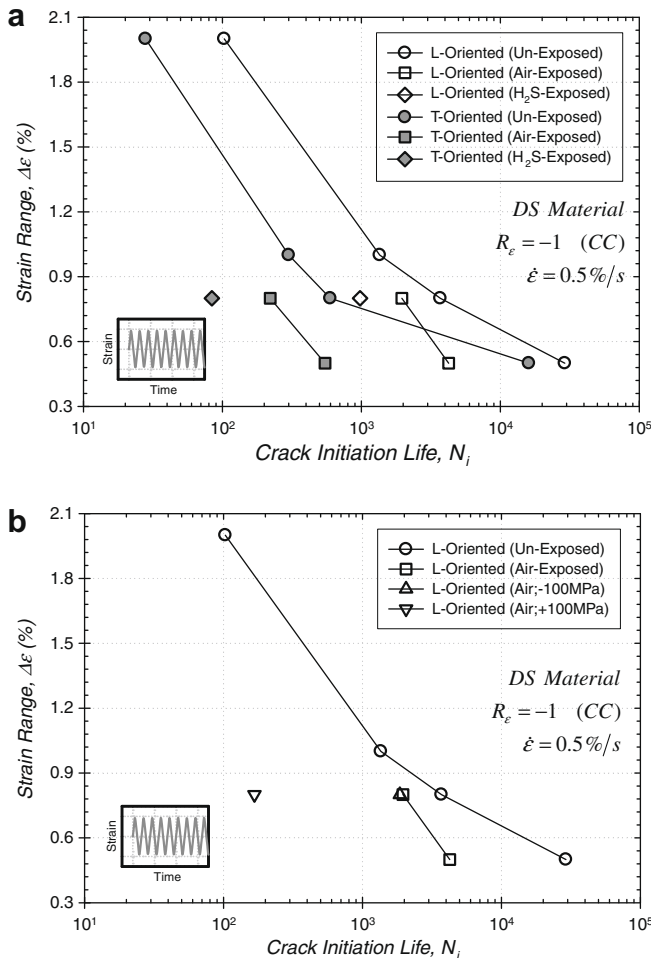


Fig. 6. Effect of pre-exposure (a) environment and (b) load on LCF crack initiation life of L- and T-oriented DS material under continuous cycling conditions with $R_e = -1$, $\dot{\epsilon} = 0.5\%/s$, and 871 °C (1600 °F). For each pre-exposed case $T = 982$ °C (1800 °F) and $t_{pre} = 100$ h.

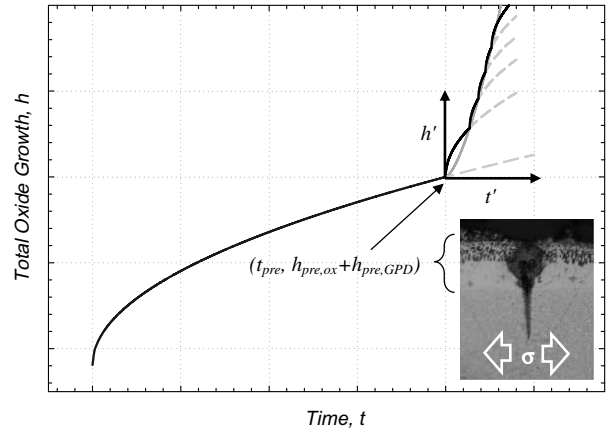


Fig. 7. Schematic of kinetics of cyclic oxide growth for pre-exposed and subsequently fatigue cycled DS material.

where h_{cr} is the final crack size and t is the total time that the sample is subjected to the pre-exposure and fatigue cycling. This relation assumes that growth kinetics during cycling and repeated rupture is merely shifted and not scaled by the pre-exposure. For unexposed cases, Eq. (3) assumes that the initial and final crack sizes are 0 and h_{cr} , respectively. For pre-exposed cases, the initial and final crack sizes are $2h_{pre}$ and h_{cr} , respectively. The analytical procedure used to derive Eq. (3) was repeated to include the high temperature pre-exposure condition

$$\frac{1}{N_i^{env}} = \frac{B_{env}}{f(\omega)} \left[\frac{\Theta_{OX} \Phi_{cc}^{env; a-\beta} (\Delta\epsilon_m)^{b+\beta}}{(h_{cr} - 2h_{pre})} \right]^{\frac{1}{\beta}} \quad (8)$$

It is assumed here that $h_{cr} > 2h_{pre}$ in all cases. For cases with $h_{cr} \leq 2h_{pre}$, the condition of the surface after pre-exposure is assumed to be extensively corroded.

Fatigue life behavior at intermediate orientations between L and T have been investigated earlier for DS Ni-base superalloys [14,23,24]. Data are generally approximated well by fourth order polynomials. As such, the term $f(\omega)$ is included to account for orientation effects. The variable ω is the angle from the DS axis of the material or specimen to the stress axis. Specifically, it is implicitly assumed that the effect of material orientation (e.g. L-versus T-oriented) is separable. For the L-orientation, $f(\omega = 0) \equiv 1.0$, and the slopes at both the L, T, and an intermediate orientation are designed to be flat, i.e., $f'(\omega = 0) = f'(\omega = \frac{\pi}{4}) = f'(\omega = \frac{\pi}{2}) = 0$. The remaining coefficients of $f(\omega)$ are determined by comparing the lives of the L- and T-oriented DS material subjected to similar conditions in which the coupled environmental-fatigue mechanism is dominant (cf. Table 3). For example, imposing the condition of air-pre-exposure with subsequent cycling at 0.8% leads $f(\omega = \frac{\pi}{2})$ after systematic elimination, e.g.

$$f(\omega = \frac{\pi}{2}) = \frac{N_i^{env}(\omega = \frac{\pi}{2}) f_{el}(\omega = 0)}{N_i^{env}(\omega = 0)} = \frac{(221)(1.0)}{(1958)} = 0.11. \quad (9)$$

Predictions of total crack initiation life of the DS material are made from combining two or more damage terms into a damage mechanism formulation similar to Miner's rule. Dominant damage is predicted based on the summed contribution of fatigue damage and coupled environmental-fatigue damage mechanisms, e.g.

$$\frac{1}{N_i|_{dom}} = \max \left\{ \frac{1}{N_i^{fat}}, \frac{1}{N_i^{env}} \right\}, \quad (10)$$

Expressions for both N_i^{fat} and N_i^{env} are relationships between crack initiation life and driving force for the corresponding damage

mode. For example, N_i^{fat} is the crack initiation life under conditions facilitating conventional fatigue failure mechanisms dominant at moderate and low temperatures [25]. Using Eqs. (8) and (10), crack initiation life predictions were made for both orientations of the subject DS material, as shown in Fig. 8. The crossover in dominant damage mechanism is easier to distinguish graphically due to the “bump” in the curve.

In each of the pre-exposed cases shown, pre-heating conditions were carried out at 982 °C. Various combinations of environment and pre-exposure times were applied. For most cases, the material was subsequently cycled at a lower temperature of 871 °C. For the L-oriented material, pre-exposure has an effect on life when the material is cycled below $\Delta\varepsilon = 1.6\%$. This threshold exists at $\Delta\varepsilon = 1.1\%$ for the T-oriented material. Amongst air and the simulated IGCC pre-exposures, the latter has the most damaging effect on life. Decreasing the duration at which a specimen is pre-exposed in air has the effect of increasing the predicted life. The upper bound on predicted life under any type on pre-exposure is the life of the unexposed material.

The predicted transitions from fatigue to environment-fatigue damage for both the L- and T-oriented material are affected the most by long term pre-exposure to the simulated IGCC environment. For identical fatigue conditions, the DS Ni-base materials are designed to exhibit material properties facilitating higher fatigue strength along the primary stress axis compared to that of the transverse axis. This is a consequence of the lower elastic modulus and high yield strength along the L-orientation.

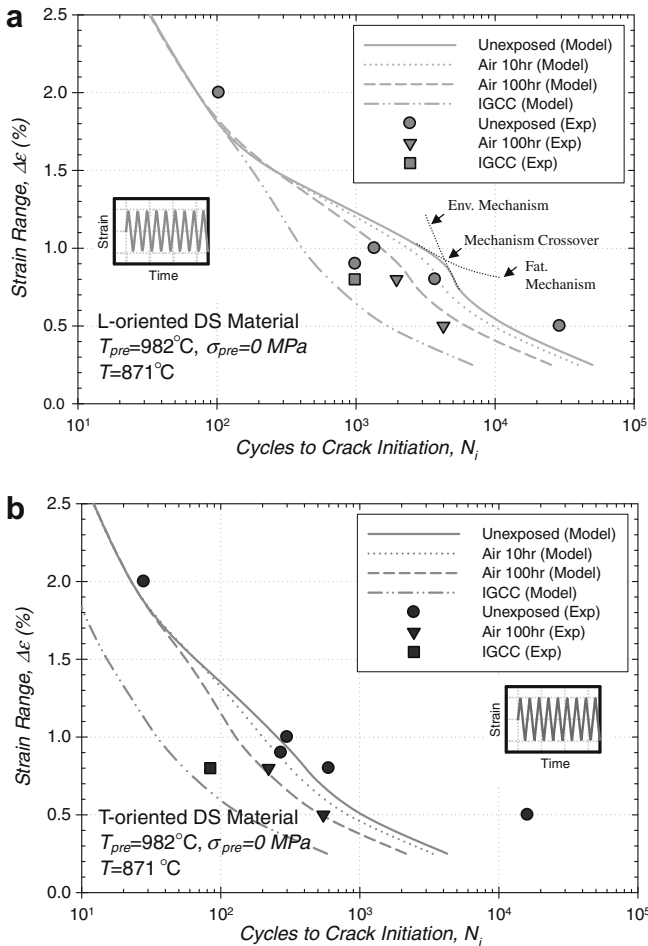


Fig. 8. Correlations of total fatigue life based on pre-exposed (a) L- and (b) T-oriented DS material under LCF conditions in air. For each case, $R_e = -1$, and $\dot{\varepsilon} = 0.5\%/s$.

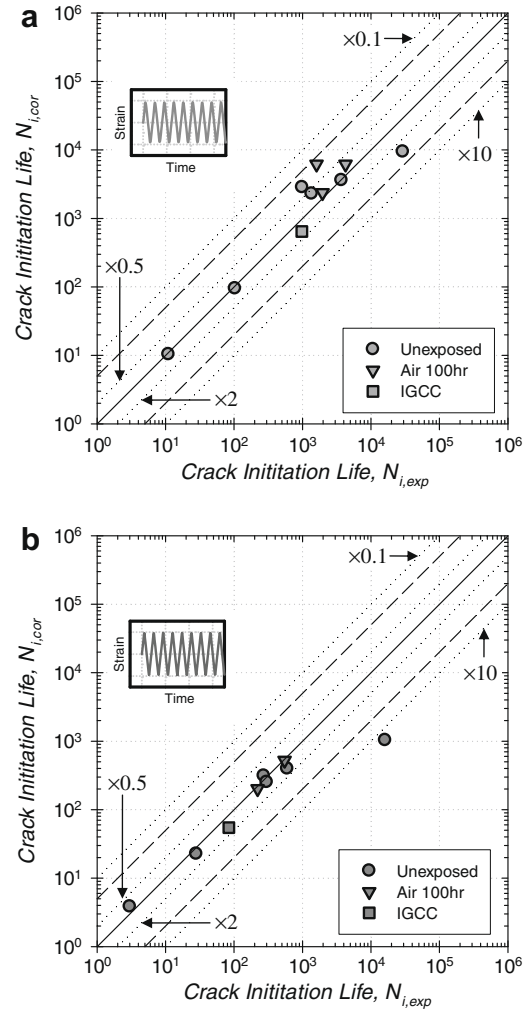


Fig. 9. Comparison of experiments (exp) and correlations (cor) for (a) L- and (b) T-oriented DS material under unexposed and pre-exposed isothermal LCF conditions. For each case $R_e = -1$, $\dot{\varepsilon}_{th} = 0$, and $\dot{\varepsilon} = 0.5\%/s$.

Crack initiation life correlations are compared with experiments in Fig. 9. The model performs well for both L- and T-oriented materials under pre-exposed conditions followed by LCF. In most cases, fatigue life of pre-exposed can be modeled accurately within a factor of 2.0. It is reasonable that the form of this model can be used to make predictions of crack initiation life for other variations of DS Ni-base superalloys (e.g. DS Mar-M247, CM247LC); however, experimental results are needed to determine the material constants in Eqs. (8) and (10). Additionally, since the L-oriented material has mechanical properties that resemble single crystal (SC) materials, this model is also applicable to SC turbine blade materials.

7. Summary

To date, the influence of thermal/mechanical pre-exposure on deformation, life, and crack initiation has not been given significant consideration in the development of fatigue crack initiation models; however, the effects of prior exposure to strain and high temperature to fatigue life are quite significant, since up to 50% of crack initiation life can be lost or gained via prior creep strain of at most 0.4% in tension or compression, respectively. The effects of prior exposure on crack initiation behavior of a DS material were investigated by pre-exposing specimens to high temperature

either in unloaded or sustained loading conditions. For the unloaded and compressively loaded cases, formation of the oxide and γ' -depleted layers allowed surface cracks to initiate very rapidly during subsequent fatigue cycling. The simulated IGCC environment (rich-in highly corrosive sulphidizing contaminants) was more detrimental to the crack initiation life than the oxidizing environment. The most detrimental pre-exposure configuration was that in which a sample was subjected to a sustained tensile load at high temperature. During subsequent loading, cracks were nucleated by coalescence of microcracks that had formed during the pre-exposure period. In either case, the damage mechanism responsible for crack initiation in the material was moderated by the pre-exposure condition. The number of cycles necessary for promoting crack initiation of pre-exposed samples was always less than that of unexposed samples. A physically based analytical model was developed to correlate the effect of stress-free surface degradation on the reduction of N_i , when coupled environmental-fatigue damage dominates. Since h_{pre} is a function of pre-exposure conditions, variables such temperature, time, and environment are included in the formulation.

Acknowledgements

The authors are grateful for the support of GE Energy Systems through the Department of Energy cooperative agreement DE-FC26-03NT41448. Ali P. Gordon is thankful for the support from the Georgia Space Grant Consortium in conducting this research.

References

- [1] EPRI. Reducing life cycle costs for gas turbine hot section components Electric Power Research Institute (EPRI), Technical Report 1014679, Palo Alto, CA; 2006.
- [2] Gordon AP. Crack initiation modeling of a directionally-solidified Ni-base superalloy. PhD Thesis, Georgia Institute of Technology, Atlanta, GA; 2006.
- [3] Boismier DA, Sehitoglu H. Thermo-mechanical fatigue of Mar-M247: part 1-experiments. *J Eng Mater Technol* 1990;112(1):68–79.
- [4] Sehitoglu H, Boismier DA. Thermo-mechanical fatigue of Mar-M247: part 2-life prediction. *J Eng Mater Technol* 1990;112(1):80–9.
- [5] Neu RW, Sehitoglu H. Thermomechanical fatigue, oxidation and creep: part I damage mechanisms. *Metallur Trans A* 1989;20:1755–67.
- [6] Neu RW, Sehitoglu H. Thermomechanical fatigue, oxidation and creep: part II life prediction. *Metallur Trans A* 1989;20:1755–67.
- [7] Miller MP, McDowell DL, Oemke RLT. A creep-fatigue-oxidation microcrack propagation model for thermomechanical fatigue. *J Eng Mater Technol* 1992;114:282–8.
- [8] Manson SS, Halford GR. Practical implementation of the double linear damage rule and damage curve approach for treating cumulative fatigue damage. *Int J Fract* 1981;17(2):169–92.
- [9] Manson SS, Halford GR. Re-examination of cumulative fatigue damage analysis – an engineering perspective. *Eng Fract Mech* 1985;25(5–6):539–71.
- [10] Kalluri S, Halford GR, McGaw MA. Prestraining and its influence on subsequent fatigue life. In: Proceedings of the 1994 third symposium on advances in fatigue lifetime predictive techniques, May 16–17 1994, Montreal, Quebec, Can, ASTM. Berlin: Springer; 1996. p. 328–41.
- [11] Rong TS, Jones IP, Smallman RE. Pre-creep strain on single crystal Ni₃Al. *Acta Mater* 1997;45(5):2139–45.
- [12] Christ H-J, Schöler K. Effect of prestraining on high-temperature fatigue behaviour of two Ni-base superalloys. *Z Metallkd* 2004;95(6):542–50.
- [13] Ott M, Mughrabi H. Dependence of the high-temperature low-cycle fatigue behavior of the monocrystalline nickel-base superalloys CMSX-4 and CMSX-6 on the γ/γ' -morphology. *Mater Sci Eng A* 1999;272:24–30.
- [14] Wright PK, Anderson AF. Influence of orientation on the fatigue of directionally solidified superalloys. In: Tien JK et al., editors, Fourth international symposium on superalloys, Seven Springs, PA, American Society for Materials; 1980. p. 689–98.
- [15] Antolovich SD, Baur R, Liu S. A mechanistically based model for high temperature LCF of Ni base superalloys. In: Tien JK, editor, Superalloys '80 (4th international symposium), Seven Springs, PA; 1980. p. 605–13.
- [16] Sajjadi SA, Nategh S. A high temperature deformation mechanism map for the high performance Ni-base superalloy GTD-111. *Mater Sci Eng A* 2001;307:158–64.
- [17] Rigdon R, Miles K. The cleaner coal option. *Power Eng Int* 2006;June–July:37–8.
- [18] Ibanez AR, Srinivasan VS, Saxena A. Creep deformation and rupture behaviour of directionally solidified GTD 111 superalloy. *Fat Fract Eng Mater Struct* 2006;29:1010–20.
- [19] Gordon AP, Trexler MD, Neu RW, McDowell DL. Corrosion kinetics of a directionally-solidified Ni-base superalloy. *Acta Mater* 2007;55(10):3375–85.
- [20] American Society for Testing and Materials. Annual book of ASTM standards, vol. 03.01. West Conshohocken, PA: ASTM International; 2007.
- [21] Trexler MD, Sanders TH, Singh PM. Automation of a McBain-Bakr-type thermogravimetric analyzer using a digital image correlation technique. *Rev Sci Instrum* 2006;77(2):025103.
- [22] Lemaitre J, Dufailly J. Modeling very low cycle fatigue. *Int J Damage Mech* 1995;4:153–70.
- [23] Marchionni M, Osinkolu GA, Maldini M. High temperature cyclic deformation of a directionally solidified Ni-base superalloy. *Fatig Fract Eng Mater Struct* 1996;19(8):955–62.
- [24] Bernhardt O-E, Mücke R. A lifetime procedure for anisotropic materials. *Commun Numer Meth Eng* 2000;16:519–27.
- [25] Gordon AP, Neu RW, McDowell DL. Fatigue-creep-environment interactions in a directionally solidified Ni-base superalloy. In: 16th European conference of fracture (ECF16), Alexandroupolis, Greece; 2006.